4

Pixel-Based Artificial Neural Networks in Computer-Aided Diagnosis

Kenji Suzuki, Ph.D.
Department of Radiology, Division of Biological Sciences,
The University of Chicago
USA

1. Introduction

Artificial neural networks (ANNs) play an essential role in the medical imaging field, including medical image analysis and computer-aided diagnosis (CAD) (Doi 2005; Giger and Suzuki 2007), because objects such as lesions and organs in medical images may not be represented accurately by a simple equation. For example, a lung nodule is generally modeled as a solid sphere, but there are nodules of various shapes and nodules with internal inhomogeneities, such as spiculated nodules and ground-glass nodules. A polyp in the colon is modeled as a bulbous object, but there are also polyps which exhibit a flat shape (Lostumbo, Wanamaker et al. 2010). Thus, diagnostic tasks in medical images essentially require "learning from examples (or data)."

One of the most popular uses of ANNs in medical image analysis is the classification of objects such as lesions into certain classes (e.g., abnormal or normal, lesions or non-lesions, and malignant or benign). The task of ANNs here is to determine "optimal" boundaries for separating classes in the multi-dimensional feature space which is formed by input features (e.g., contrast, area, and circularity) obtained from object candidates. Machine-learning algorithms for classification include linear discriminant analysis (Fukunaga 1990), quadratic discriminant analysis (Fukunaga 1990), multilayer perceptron (Rumelhart, Hinton et al. 1986), and support vector machines (Vapnik 1995). Such machine-learning algorithms were applied to lung nodule detection in chest radiography (Shiraishi, Li et al. 2006) and thoracic CT (Armato, Giger et al. 2001; Arimura, Katsuragawa et al. 2004), classification of lung nodules into benign or malignant in chest radiography (Aoyama, Li et al. 2002) and thoracic CT (Aoyama, Li et al. 2003), detection of microcalcifications in mammography (Wu, Doi et al. 1992), classification of masses into benign or malignant in mammography (Huo, Giger et al. 1998), polyp detection in CT colonography (Yoshida and Nappi 2001; Jerebko, Summers et al. 2003), determining subjective similarity measure of mammographic images (Muramatsu, Li et al. 2005; Muramatsu, Li et al. 2006; Muramatsu, Li et al. 2007), and detection of aneurysms in brain MRI (Arimura, Li et al. 2006).

Recently, as available computational power increased dramatically, pixel/voxel-based ANNs (PANNs) emerged in medical image processing/analysis which use pixel/voxel values in images directly instead of features calculated from segmented regions as input

information; thus, feature calculation or segmentation is not required. Because the PANN can avoid errors caused by inaccurate feature calculation and segmentation, the performance of the PANN can potentially be higher than that of common classifiers. In this chapter, PANNs are surveyed and reviewed to make clear a) classes of PANNs, b) the similarities and differences within different PANNs and those between PANNs and ordinary classifiers, c) the advantages and limitations of PANNs, and d) their applications in medical imaging.

2. Pixel/voxel-based Artificial Neural Network (PANN)

2.1 Overview

PANNs have been developed for tasks in medical image processing/analysis and computer vision. Table 1 summarizes classes of PANNs, their functions, and their applications. There are three classes of PANNs: neural filters (Suzuki, Horiba et al. 2002; Suzuki, Horiba et al. 2002) (including neural edge enhancers (Suzuki, Horiba et al. 2003; Suzuki, Horiba et al. 2004)), convolution neural networks (NNs) (Lo, Lou et al. 1995; Lo, Chan et al. 1995; Lin, Lo et al. 1996; Sahiner, Chan et al. 1996; Lawrence, Giles et al. 1997; Neubauer 1998; Lo, Li et al. 2002) (including shift-invariant NNs (Zhang, Doi et al. 1994; Wei, Nishikawa et al. 1996; Zhang, Doi et al. 1996)), and massive-training ANNs (MTANNs) (Suzuki, Armato et al. 2003; Suzuki, Abe et al. 2006; Suzuki, Yoshida et al. 2006; Oda, Awai et al. 2009; Suzuki 2009) (including multiple MTANNs (Suzuki, Horiba et al. 2002; Suzuki, Horiba et al. 2002; Suzuki, Armato et al. 2003; Arimura, Katsuragawa et al. 2004; Suzuki, Li et al. 2005; Suzuki, Shiraishi et al. 2005), a mixture of expert MTANNs (Suzuki, Yoshida et al. 2008; Suzuki, Rockey et al. 2010), a multi-resolution MTANN (Suzuki, Abe et al. 2006), a Laplacian eigenfunction MTANN (LAP-MTANN) (Suzuki, Zhang et al. in press), and a massive-training support vector regression (MTSVR) (Xu and Suzuki 2010 (in press))). The class of neural filters has been used for image-processing tasks such as edge-preserving noise reduction in radiographs and other digital pictures (Suzuki, Horiba et al. 2002; Suzuki, Horiba et al. 2002), edge enhancement from noisy images (Suzuki, Horiba et al. 2003), and enhancement of subjective edges traced by a physician in left ventriculograms (Suzuki, Horiba et al. 2004). The class of convolution NNs has been applied to classification tasks such as false-positive (FP) reduction in CAD schemes for detection of lung nodules in chest radiographs (CXRs) (Lo, Lou et al. 1995; Lo, Chan et al. 1995; Lin, Lo et al. 1996), FP reduction in CAD schemes for detection of microcalcifications (Lo, Li et al. 2002) and masses (Sahiner, Chan et al. 1996) in mammography, face recognition (Lawrence, Giles et al. 1997), and character recognition (Neubauer 1998). The class of MTANNs has been used for classification, such as FP reduction in CAD schemes for detection of lung nodules in CXR (Suzuki, Shiraishi et al. 2005) and CT (Suzuki, Armato et al. 2003; Arimura, Katsuragawa et al. 2004; Li, Arimura et al. 2005), distinction between benign and malignant lung nodules in CT (Suzuki, Li et al. 2005), and FP reduction in a CAD scheme for polyp detection in CT colonography (Suzuki, Yoshida et al. 2006; Suzuki, Yoshida et al. 2008; Suzuki, Rockey et al. 2010; Xu and Suzuki 2010 (in press); Suzuki, Zhang et al. in press). The MTANNs have also been applied to pattern enhancement and suppression such as separation of bone from soft tissue in CXR (Suzuki, Abe et al. 2006; Oda, Awai et al. 2009), and enhancement of lung nodules in CT (Suzuki 2009).

PANNs	Functions	Applications
Neural filters (including neural edge enhancers)	Image processing	Edge-preserving noise reduction [20, 21]. Edge enhancement from noisy images [22]. Enhancement of subjective edges traced by a physician [23].
Convolution neural networks (including shift-invariant neural networks)	Classification	FP reduction in CAD for lung nodule detection in CXR [24-26]. FP reduction in CAD for detection of microcalcifications [27] and masses [28] in mammography. Face recognition [29]. Character recognition [30].
Massive-training artificial neural networks (MTANNs, including a mixture of expert MTANNs, and a LAP-MTANN)	Classification (image processing + scoring), pattern enhancement and suppression, object detection (pattern enhancement followed by thresholding or segmentation),	FP reduction in CAD for detection of lung nodules in CXR [39] and CT [9, 34, 45]. Distinction between benign and malignant lung nodules in CT [40]. FP reduction in CAD for polyp detection in CT colonography [35, 41-44]. Bone separation from soft tissue in CXR [36, 37]. Enhancement of lung nodules in CT [38].

Table 1. Classes of PANNs, their functions, and their applications

2.2 Neural filters

In the field of signal/image processing, supervised nonlinear filters based on a multilayer ANN, called neural filters, have been studied (Suzuki, Horiba et al. 2002; Suzuki, Horiba et al. 2002). The neural filter employs a linear-output ANN model as a convolution kernel of a filter. The inputs to the neural filter are an object pixel value and spatially/spatiotemporally adjacent pixel values in a subregion (or local window). The output of the neural filter is a single pixel value. The neural filter is trained with input images and corresponding "teaching" (desired or ideal) images. The training is performed by a linear-output back-propagation algorithm which is a back-propagation algorithm modified for the linear-output ANN architecture. Neural filters can acquire the functions of various linear and nonlinear filtering through training. Neural filters have been applied to reduction of the

quantum noise in x-ray fluoroscopic and radiographic images (Suzuki, Horiba et al. 2002; Suzuki, Horiba et al. 2002). It was reported that the performance of the neural filter was superior to that of well-known nonlinear filters such as an adaptive weighted averaging filter (Ozkan, Sezan et al. 1993). A study (Suzuki, Horiba et al. 2002) showed that adding features from the subregion to the input information improved the performance of the neural filter. Neural filters have been extended to accommodate the task of enhancement of edges, and a supervised edge enhancer (detector), called a neural edge enhancer, was developed (Suzuki, Horiba et al. 2003). The neural edge enhancer can acquire the function of a desired edge enhancer through training. It was reported that the performance of the neural edge enhancer in the detection of edges from noisy images was far superior to that of well-known edge detectors such as the Canny edge detector (Canny 1986), the Marr-Hildreth edge detector (Marr and Hildreth 1980), and the Huckel edge detector (Hueckel 1971). In its application to the contour extraction of the left ventricular cavity in digital angiography, it has been reported that the neural edge enhancer can accurately replicate the subjective edges traced by a cardiologist (Suzuki, Horiba et al. 2004).

2.3 Massive-Training Artificial Neural Network (MTANN)

An MTANN was developed by extension of neural filters to accommodate various pattern-recognition tasks (Suzuki, Armato et al. 2003). A two-dimensional (2D) MTANN was first developed for distinguishing a specific opacity (pattern) from other opacities (patterns) in 2D images (Suzuki, Armato et al. 2003). The 2D MTANN was applied to reduction of FPs in computerized detection of lung nodules on 2D CT slices in a slice-by-slice way (Suzuki, Armato et al. 2003; Arimura, Katsuragawa et al. 2004; Li, Arimura et al. 2005) and in CXR (Suzuki, Shiraishi et al. 2005), the separation of ribs from soft tissue in CXR (Suzuki, Abe et al. 2006; Oda, Awai et al. 2009), and the distinction between benign and malignant lung nodules on 2D CT slices (Suzuki, Li et al. 2005). For processing of three-dimensional (3D) volume data, a 3D MTANN was developed by extending the structure of the 2D MTANN, and it was applied to 3D CT colonography data (Suzuki, Yoshida et al. 2006; Suzuki, Yoshida et al. 2008; Suzuki, Rockey et al. 2010; Xu and Suzuki 2010 (in press); Suzuki, Zhang et al. in press).

The generalized architecture of an MTANN which unifies 2D and 3D MTANNs is shown in Fig. 1. An MTANN consists of an ANN model such as a linear-output ANN regression model and a support vector regression model, which is capable of operating on pixel/voxel data directly (Suzuki, Horiba et al. 2003). The linear-output ANN regression model employs a linear function instead of a sigmoid function as the activation function of the unit in the output layer because the characteristics of an ANN were improved significantly with a linear function when applied to the continuous mapping of values in image processing (Suzuki, Horiba et al. 2003). Note that the activation functions of the units in the hidden layer are a sigmoid function for nonlinear processing, and those of the unit in the input layer are an identity function, as usual. The pixel/voxel values of the input images/volumes may be normalized from 0 to 1. The input to the MTANN consists of pixel/voxel values in a subregion/sub-volume, R, extracted from an input image/volume. The output of the MTANN is a continuous scalar value, which is associated with the center voxel in the subregion, and is represented by

$$O(x, y, z \text{ or } t) = NN\{I(x-i, y-j, z-k \text{ or } t-k) \mid (i, j, k) \in R\}, \quad (1)$$

where x, y, and z or t are the coordinate indices, $NN(\cdot)$ is the output of the ANN model, and $I(x,y,z \text{ or } t)$ is a pixel/voxel value of the input image/volume. The entire output image/volume is obtained by scanning with the input subvolume of the MTANN on the entire input image/volume. The input subregion/subvolume and the scanning with the MTANN can be analogous to the kernel of a convolution filter and the convolutional operation of the filter, respectively.

The MTANN is trained with input images/volumes and the corresponding "teaching" images/volumes for enhancement of a specific pattern and suppression of other patterns in images/volumes. The "teaching" images/volumes are ideal or desired images for the corresponding input images/volumes. For enhancement of lesions and suppression of non-lesions, the teaching volume contains a map for the "likelihood of being lesions.

To enrich the training samples, a training region, R_T, extracted from the input images is divided pixel by pixel into a large number of overlapping subregions. Single pixels are extracted from the corresponding teaching images as teaching values. The MTANN is massively trained by use of each of a large number of input subregions together with each of the corresponding teaching single pixels; hence the term "massive-training ANN." The error to be minimized by training of the MTANN is represented by

$$E = \frac{1}{P}\sum_{c}\sum_{(x,y,z\text{or}t)\in R_T}\left\{T_c(x,y,z\text{or}t) - O_c(x,y,z\text{or}t)\right\}^2, \tag{2}$$

where c is a training case number, O_c is the output of the MTANN for the c^{th} case, T_c is the teaching value for the MTANN for the c^{th} case, and P is the number of total training voxels in the training region for the MTANN, R_T. The expert 3D MTANN is trained by a linear-output back-propagation (BP) algorithm (Suzuki, Horiba et al. 2003) which was derived for the linear-output ANN model by use of the generalized delta rule (Rumelhart, Hinton et al. 1986). After training, the MTANN is expected to output the highest value when a lesion is located at the center of the subregion of the MTANN, a lower value as the distance from the subregion center increases, and zero when the input subregion contains a non-lesion.

A scoring method is used for combining output pixels from the trained MTANNs. A score for a given region of interest (ROI) from the MTANN is defined as

$$S = \sum_{(x,y,z\text{or}t)\in R_E} f_W\left(x,y,z\text{or}t\right)\times O\left(x,y,z\text{or}t\right), \tag{3}$$

where f_W is a weighting function for combining pixel-based output responses from the trained MTANN into a single score, which may often be the same distribution function used in the teaching images, and with its center corresponding to the center of the region for evaluation, R_E; and O is the output image of the trained MTANN, where its center corresponds to the center of R_E. This score represents the weighted sum of the estimates for the likelihood that the ROI (e.g., a lesion candidate) contains a lesion near the center, i.e., a higher score would indicate a lesion, and a lower score would indicate a non-lesion. Thresholding is then performed on the scores for distinction between lesions and non-lesions.

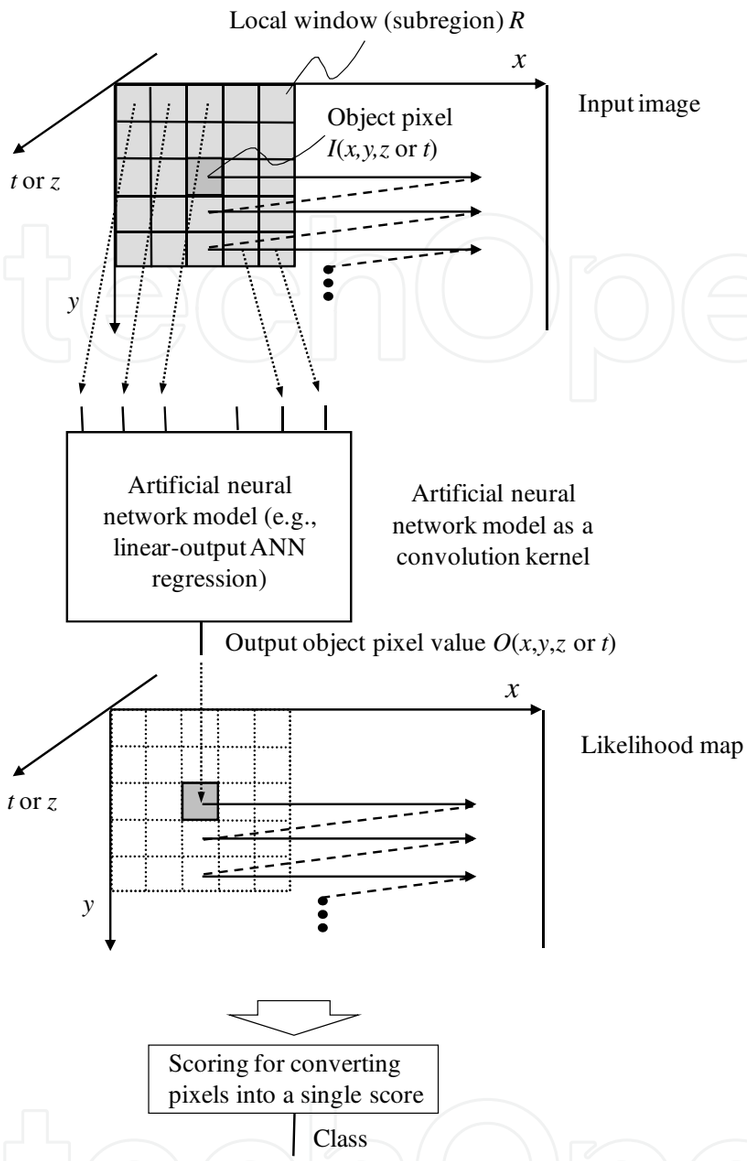

Fig. 1. Generalized architecture of an MTANN consisting of an ANN model (e.g., linear-output ANN regression and support vector regression) with sub-region input and single-pixel output. All pixel values in a sub-region extracted from an input image are entered as input to the ANN model. The ANN model outputs a single pixel value for each sub-region, the location of which corresponds to the center pixel in the sub-region. Output pixel value is mapped back to the corresponding pixel in the output image.

2.4 Convolution Neural Network (NN)

A convolution NN has first been proposed for handwritten ZIP-code recognition (LeCun, Boser et al. 1989). The architecture of a convolution NN is illustrated in Fig. 2. The convolution NN can be considered as a simplified version of the Neocognitron model which was proposed to simulate the human visual system in 1980 (Fukushima 1980). The input and output of the convolution NN are images and nominal class labels, respectively. The

convolution NN consists of one input layer, several hidden layers, and one output layer. The layers are connected with local shift-invariant inter-connections (or convolution with a local kernel). Unlike the Neocognitron, the convolution NN has no lateral interconnections or feedback loops, and the error BP algorithm (Rumelhart, Hinton et al. 1986) is used for training of the convolution NN. Units (neurons) in any hidden layer are organized in groups. Each unit in a subsequent layer is connected with the units of a small region in each group in the preceding layer. The groups between adjacent layers are interconnected by weights that are organized in kernels. For obtaining the shift-invariant responses, connection weights between any two groups in two layers are constrained to be shift-invariant; in other words, forward signal propagation is similar to a shift-invariant convolution operation. The signals from the units in a certain layer are convolved with the weight kernel, and the resulting value of the convolution is collected into the corresponding unit in the subsequent layer. This value is further processed by the unit through an activation function and produces an output signal. The activation function between two layers is a sigmoid function. For deriving the training algorithm for the convolution NN, the generalized delta rule (Rumelhart, Hinton et al. 1986) is applied to the architecture of the convolution NN. For distinguishing an ROI containing a lesion from an ROI containing a non-lesion, a class label (e.g., 1 for a lesion, 0 for a non-lesion) is assigned to an output unit.
Variants of the convolution NN have been proposed. The dual-kernel approach, which employs central kernels and peripheral kernels in each layer (Lo, Chan et al. 1995), was proposed for distinction between lung nodules and non-nodules in chest radiographs (Lo, Lou et al. 1995; Lo, Chan et al. 1995) and distinction between microcalcifications and other anatomic structures in mammograms (Lo, Chan et al. 1995). This dual-kernel-based convolution NN has several output units (instead of one or two output units in the standard convolution NN) for two-class classification. The fuzzy association was employed for transformation of output values from the output units to two classes (i.e., nodules or non-nodules; microcalcifications or other anatomic structures). A convolution NN which has subsampling layers has been developed for face recognition (Lawrence, Giles et al. 1997).

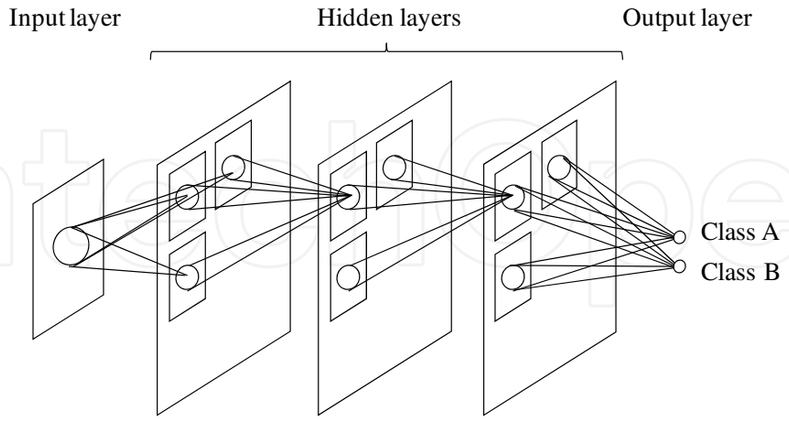

Fig. 2. Architecture of a convolution NN. The convolution NN can be considered as a simplified version of the Neocognitron model, which was proposed to simulate the human visual system. The layers in the convolution NN are connected with local shift-invariant inter-connections (or convolution with a local kernel). The input and output of the convolution NN are images and nominal class labels (e.g., Class A and Class B), respectively.

Some convolution NNs have one output unit (Neubauer 1998; Gurcan, Sahiner et al. 2001), some have two output units (Chan, Lo et al. 1995), and some have more than two output units (Lo, Lou et al. 1995; Lo, Chan et al. 1995; Lawrence, Giles et al. 1997; Lo, Li et al. 2002) for two-class classification.

Shift-invariant NNs (Zhang, Doi et al. 1994; Zhang, Doi et al. 1996) are mostly the same as convolution NNs except for the output layer, which outputs images instead of classes. The shift-invariant NNs were used for localization (detection) of lesions in images, for example, detection of microcalcifications in mammograms (Zhang, Doi et al. 1994; Zhang, Doi et al. 1996), and detection of the boundaries of the human corneal endothelium in photomicrographs (Hasegawa, Itoh et al. 1996).

2.5 Non-PANN – Feature-based classifiers

One of most popular uses of ANNs would probably be classification. In this use, an ANN is called a classifier. A standard classification approach based on a multilayer perceptron is illustrated in Fig. 3. First, target objects are segmented by use of a segmentation method. Next, features are extracted from the segmented objects. Then, extracted features are entered as input to an ANN model such as linear discriminant analysis (Fukunaga 1990), quadratic

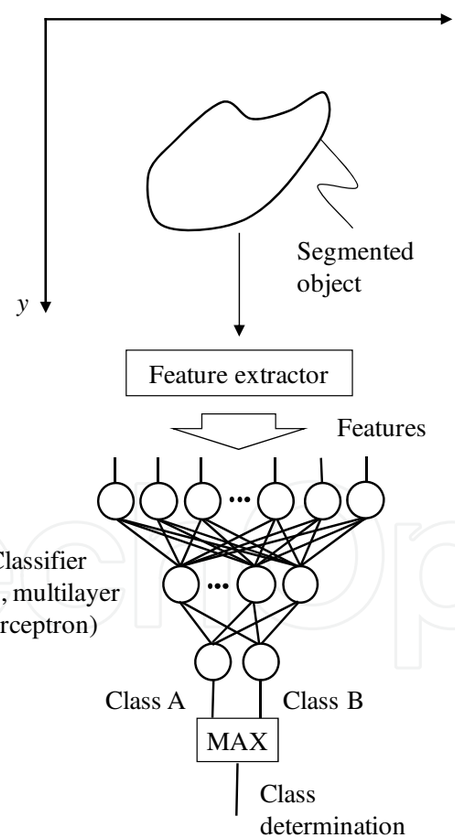

Fig. 3. Standard classifier approach to classification of an object. Features (e.g., contrast, effective diameter, and circularity) are extracted from a segmented object in an image. Those features are entered as input to a classifier such as a multilayer perceptron. Class determination is made by taking the class of the output unit with the maximum value.

discriminant analysis (Fukunaga 1990), a multilayer perceptron (Rumelhart, Hinton et al. 1986), and a support-vector machine (Vapnik 1995). The ANN model is trained with sets of input features and correct class labels. A class label of 1 is assigned to the corresponding output unit when a training sample belongs to that class, and 0 is assigned to the other output units. After training, the class of the unit with the maximum value is determined to be the corresponding class to which an unknown sample belongs. For details of feature-based classifiers, refer to one of many textbooks in pattern recognition such as (Rumelhart, Hinton et al. 1986; Fukunaga 1990; Bishop 1995; Vapnik 1995)

3. Similarities and differences

3.1 Within different PANN algorithms

MTANNs (Suzuki, Armato et al. 2003) were developed by extension of neural filters to accommodate various pattern-recognition tasks. In other words, neural filters are a subclass or a special case of MTANNs. The applications and functions of neural filters are limited to noise reduction (Suzuki, Horiba et al. 2002; Suzuki, Horiba et al. 2002) and edge enhancement (Suzuki, Horiba et al. 2003; Suzuki, Horiba et al. 2004), whereas those of MTANNs were extended to include classification (Suzuki, Armato et al. 2003; Suzuki, Li et al. 2005; Suzuki, Shiraishi et al. 2005; Suzuki, Abe et al. 2006; Suzuki, Yoshida et al. 2006; Suzuki, Yoshida et al. 2008; Suzuki, Rockey et al. 2010; Xu and Suzuki 2010 (in press); Suzuki, Zhang et al. in press), pattern enhancement and suppression (Suzuki, Abe et al. 2006), and object detection (Suzuki 2009). The input information to MTANNs, which is the pixel values in a subregion, is the same as that to neural filters. However, the output of (thus, teacher for) neural filters is the desired pixel values in a given image, whereas that of MTANNs is a map for the likelihood of being a specific pattern in a given image.

Both convolution NNs and the perceptron used for character recognition are in the class of PANN. Input information to the convolution NNs and the perceptron is the pixel values in a given image, whereas the output of (thus, teacher for) both algorithms is a nominal class label for the given image. Thus, the input and output information are the same for both algorithms. However, the input images for the perceptron for character recognition are limited to be binary, although the perceptron itself is capable of processing gray-scale images. The major difference between convolution NNs and the perceptron used for character recognition is their internal architectures. Units in layers of the perceptron are fully connected, whereas the connections in the convolution NN are spatially (locally) limited. Because of this architecture, forward signal propagation in the convolution NN is realized by a convolution operation. This convolution operation offers a shift-invariant property which is desirable for image classification. The applications and functions of the perceptron are limited to character recognition such as zip code recognition and optical character recognition, whereas those of convolution NNs are general classification of images into known classes such as classification of lesion candidates into lesions or non-lesions (Lo, Lou et al. 1995; Lo, Chan et al. 1995; Lin, Lo et al. 1996; Sahiner, Chan et al. 1996; Lo, Li et al. 2002), classification of faces (Lawrence, Giles et al. 1997), and classification of characters (Neubauer 1998).

Shift-invariant NNs are mostly the same as convolution NNs except for the output layer, which outputs images instead of classes. The shift-invariant NNs can be used for localization (detection) of objects in images in addition to classification (Zhang, Doi et al. 1994; Zhang, Doi et al. 1996).

Convolution NNs, shift-invariant NNs, and MTANNs perform convolution operations. In convolution NNs and shift-invariant NNs, convolution operations are performed within the network, as shown in Fig. 2, whereas the convolutional operation is performed outside the network in the MTANN, as show in Fig. 1.

3.2 Between PANN algorithms and ordinary classifiers

The major difference between PANNs and ordinary classifiers (i.e., feature-based classifiers) is the input information. Ordinary classifiers use features extracted from a segmented object in a given image, whereas PANNs use pixel values in a given image as the input information. Although the input information to PANNs can be features (see addition of features to the input information to neural filters in (Suzuki, Horiba et al. 2002), for example), these features are obtained pixel by pixel (rather than by object). In other words, features for PANNs are features at each pixel in a given image, whereas features for ordinary classifiers are features from a segmented object. In that sense, feature-based classifiers may be referred to as object-based classifiers. Because PANNs use pixel/voxel values in images directly instead of features calculated from segmented objects as the input information, feature calculation or segmentation is not required. Although the development of segmentation techniques has been studied for a long time, segmentation of objects is still challenging, especially for complicated objects, subtle objects, and objects in a complex background. Thus, segmentation errors may occur for complicated objects. Because with PANNs, errors caused by inaccurate feature calculation and segmentation can be avoided, the performance of PANNs can be higher than that of ordinary classifiers for some cases, such as complicated objects.

The output information from ordinary classifiers, convolution NNs, and the perceptron used for character recognition is nominal class labels, whereas that from neural filters, MTANNs, and shift-invariant NNs is images. With the scoring method in MTANNs, output images of the MTANNs are converted to likelihood scores for distinguishing among classes, which allow MTANNs to do classification. In addition to classification, MTANNs can perform pattern enhancement and suppression as well as object detection, whereas the other PANNs cannot.

4. Applications of PANN algorithms in medical images

4.1 Bone separation from soft tissue in chest radiographs (CXRs) by use of MTANNs

CXR is the most frequently used diagnostic imaging examination for chest diseases such as lung cancer, tuberculosis, and pneumonia. More than 9 million people worldwide die annually from chest diseases (Murray and Lopez 1997). Lung cancer causes 945,000 deaths, and is the leading cause of cancer deaths in the world (Murray and Lopez 1997) and in countries such as the United States, the United Kingdom, and Japan (Goodman 2002). Lung nodules (i.e., potential lung cancers) in CXR, however, can be overlooked by radiologists in from 12 to 90% of cases that have nodules visible in retrospect (Austin, Romney et al. 1992; Shah, Austin et al. 2003). Studies showed that 82 to 95% of the missed lung cancers were partly obscured by overlying bones such as ribs and/or a clavicle (Austin, Romney et al. 1992; Shah, Austin et al. 2003). To address this issue, dual-energy imaging has been investigated (Glocker and Frohnmayer 1925; Jacobson and Mackay 1958). Dual-energy imaging uses the energy dependence of the x-ray attenuation by different materials; it can

produce two tissue-selective images, i.e., a "bone" image and a "soft-tissue" image (Ishigaki, Sakuma et al. 1986; Ishigaki, Sakuma et al. 1988; Stewart and Huang 1990). Major drawbacks of dual-energy imaging, however, are that (a) the radiation dose can be double, (b) specialized equipment for obtaining dual-energy x-ray exposures is required, and (c) the subtraction of two-energy images causes an increased noise level in the images.

For resolving the above drawbacks with dual-energy images, MTANNs have been developed as an image-processing technique for separation of ribs from soft tissue (Suzuki, Abe et al. 2006). The basic idea is to train the MTANN with soft-tissue and bone images acquired with a dual-energy radiography system. For separation of ribs from soft tissue, the MTANN was trained with input CXRs and the corresponding "teaching" dual-energy bone images, as illustrated in Fig. 4 (a). Figure 4 (b) shows a non-training original CXR and a soft-tissue image obtained by use of the trained MTANN. The contrast of ribs is suppressed substantially in the MTANN soft-tissue image, whereas the contrast of soft tissue such as lung vessels is maintained.

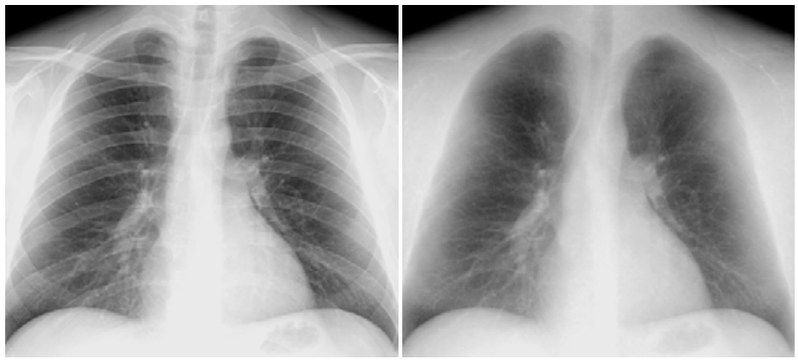

Input chest radiograph "Teaching" dual-energy soft-tissue image

(a)

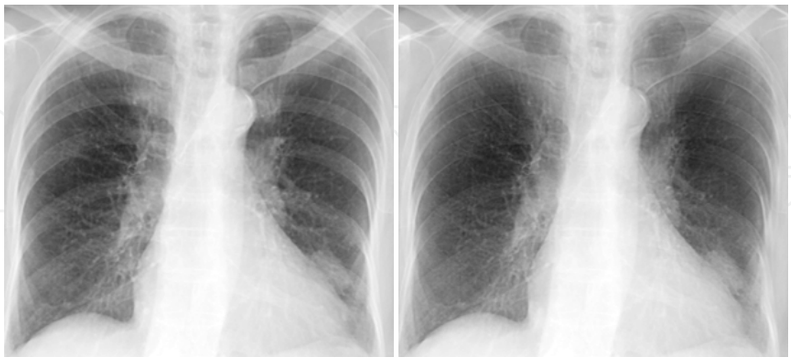

Original chest radiograph Soft-tissue image by the trained MTANN

(b)

Fig. 4. Separation of bones from soft tissue in CXRs by use of an MTANN. (a) Images used for training the MTANN. (b) Result of an application of the trained MTANN to a non-training CXR.

4.2 Enhancement and detection of lesions by use of MTANNs

Computer-aided diagnosis (CAD) has been an active area of study in medical image analysis (Doi 2005; Giger 2005; Doi 2007; Giger and Suzuki 2007). Some CAD schemes employ a filter for enhancement of lesions as a preprocessing step for improving sensitivity and specificity; but some do not employ such a filter. The filter enhances objects similar to a model employed in the filter; e.g., a blob-enhancement filter based on the Hessian matrix enhances sphere-like objects (Frangi, Niessen et al. 1999). Actual lesions, however, often differ from a simple model, e.g., a lung nodule is generally modeled as a solid sphere, but there are nodules of various shapes and inhomogeneous nodules such as nodules with spiculation and ground-glass nodules. Thus, conventional filters often fail to enhance such actual lesions.

To address this issue, a "lesion-enhancement" filter based on MTANNs has been developed for enhancement of actual lesions in a CAD scheme for detection of lung nodules in CT (Suzuki 2009). For enhancement of lesions and suppression of non-lesions in CT images, the teaching image contains a map for the "likelihood of being lesions." For enhancement of a nodule in an input CT image, a 2D Gaussian distribution was placed at the location of the nodule in the teaching image, as a model of the likelihood of being a lesion. For testing of the performance, the trained MTANN was applied to non-training lung CT images. As shown in Fig. 5, the nodule is enhanced in the output image of the trained MTANN filter, while normal structures such as lung vessels are suppressed. Note that small remaining regions due to vessels can easily be separated from nodules by use of their area information which can be obtained by use of connected-component labeling (Suzuki, Horiba et al. 2003; He, Chao et al. 2008; He, Chao et al. 2009).

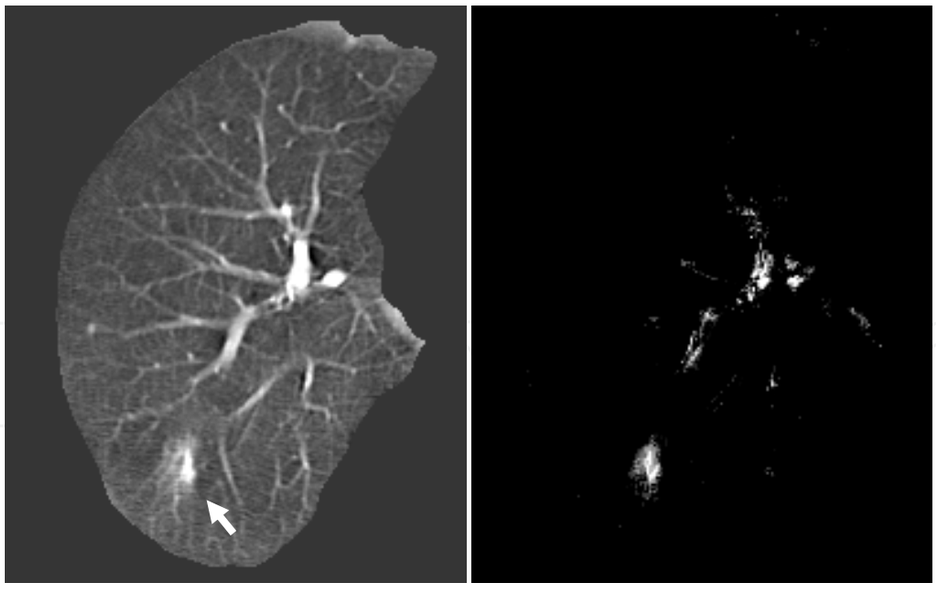

Input chest CT image with a nodule (arrow)

Output image of the trained supervised MTANN filter

Fig. 5. Enhancement of a lesion by use of the trained lesion-enhancement MTANN filter for a non-training case. (a) Original chest CT image of the segmented lung with a nodule (indicated by an arrow). (b) Output image of the trained lesion-enhancement MTANN filter.

4.3 Classification between lesions and non-lesions by use of different PANN Algorithms

1. MTANNs

A major challenge in CAD development is to reduce the number of FPs, because there are various normal structures similar to lesions in medical images. To address this issue, an FP-reduction technique based on an MTANN has been developed for a CAD scheme for lung nodule detection in CT (Suzuki, Armato et al. 2003). For enhancement of nodules (i.e., true positives) and suppression of non-nodules (i.e., FPs) on CT images, the teaching image contains a distribution of values that represent the "likelihood of being a nodule." For example, the teaching volume contains a 3D Gaussian distribution with standard deviation σ_T for a lesion and zero (i.e., completely dark) for non-lesions, as illustrated in Fig. 6. This distribution represents the "likelihood of being a lesion":

$$T(x,y,z\,or\,t)=\begin{cases}\dfrac{1}{\sqrt{2\pi}\sigma_T}\exp\left\{-\dfrac{(x^2+y^2+z^2\,or\,t^2)}{2{\sigma_T}^2}\right\} & for\ a\ lesion\\ 0 & otherwise.\end{cases} \tag{4}$$

A 3D Gaussian distribution is used to approximate an average shape of lesions. The MTANN involves training with a large number of subvolume-voxel pairs, which is called a massive-subvolumes training scheme.

A scoring method is used for combining of output voxels from the trained MTANNs. A score for a given ROI from the MTANN is defined as

$$S=\sum_{(x,y,z\,or\,t)\in R_E} f_W\left(x,y,z\,or\,t\right)\times O\left(x,y,z\,or\,t\right), \tag{5}$$

where

$$f_W\left(x,y,z\,or\,t\right)=f_G\left(x,y,z\,or\,t;\sigma\right)=\frac{1}{\sqrt{2\pi}\sigma}e^{-\frac{x^2+y^2+z^2\,or\,t^2}{2\sigma^2}} \tag{6}$$

is a 3D Gaussian weighting function with standard deviation σ, and with its center corresponding to the center of the volume for evaluation, R_E; and O is the output image of the trained MTANN, where its center corresponds to the center of R_E. The use of the 3D Gaussian weighting function allows us to combine the responses (outputs) of a trained MTANN as a 3D distribution. A 3D Gaussian function is used for scoring, because the output of a trained MTANN is expected to be similar to the 3D Gaussian distribution used in the teaching images. This score represents the weighted sum of the estimates for the likelihood that the ROI (lesion candidate) contains a lesion near the center, i.e., a higher score would indicate a lesion, and a lower score would indicate a non-lesion. Thresholding is then performed on the scores for distinction between lesions and non-lesions.

An MTANN was trained with typical nodules and typical types of FPs (non-nodules) and corresponding teaching images. The trained MTANN was applied to 57 true positives (nodules) and 1,726 FPs (non-nodules) produced by a CAD scheme (Suzuki, Armato et al.

2003). Figure 7 shows various types of nodules and non-nodules and the corresponding output images of the trained MTANN. Nodules such as a solid nodule, a part-solid (mixed-ground-glass) nodule, and a non-solid (ground-glass) nodule are enhanced, whereas non-nodules such as different-sized lung vessels and soft-tissue opacity are suppressed around the centers of ROIs. For combining output pixels into a single score for each nodule candidate, a scoring method was applied to the output images for distinction between a nodules and a non-nodule. Thresholding of scores was done for classification of nodule candidates into nodules or non-nodules. Free-response receiver operating characteristic (FROC) analysis (Bunch, Hamilton et al. 1978) was carried out for evaluation of the performance of the trained MTANN. The FROC curve for the MTANN indicates 80.3% overall sensitivity (100% classification performance) and a reduction in the FP rate from 0.98 to 0.18 per section, as shown in Fig. 8.

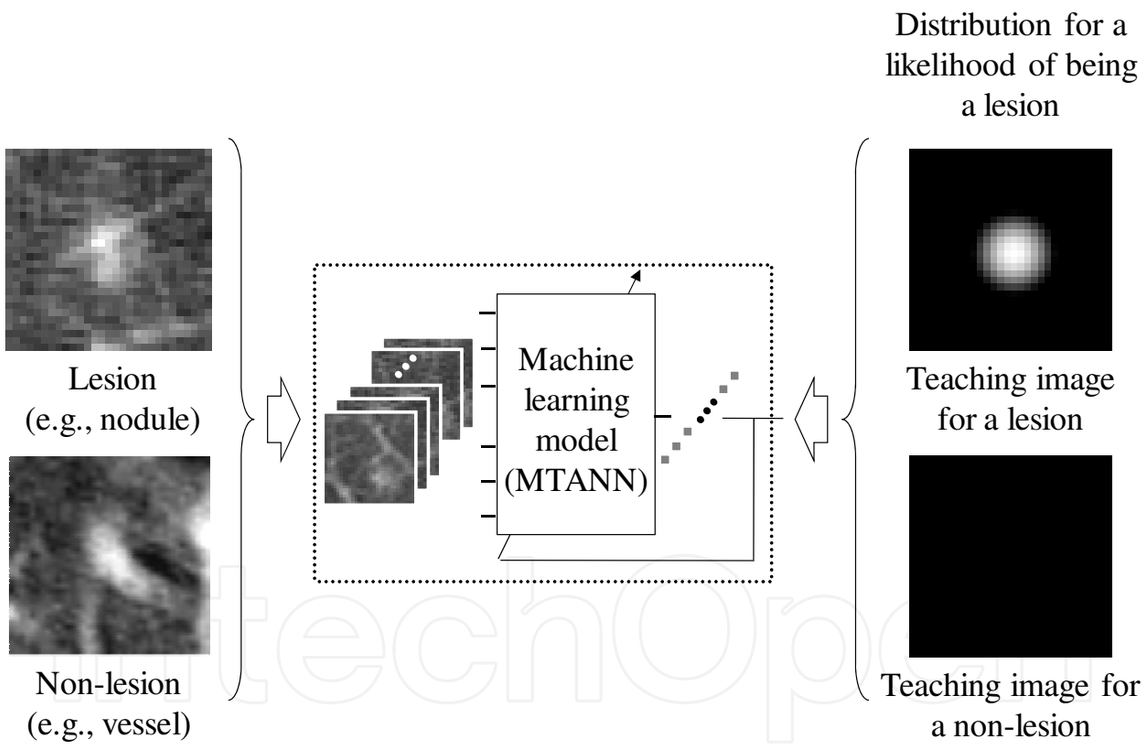

Fig. 6. Training of an MTANN for distinction between lesions and non-lesions in a CAD scheme for detection of lesions in medical images. The teaching image for a lesion contains a Gaussian distribution; that for a non-lesion contains zero (completely dark). After the training, the MTANN expects to enhance lesions and suppress non-lesions.

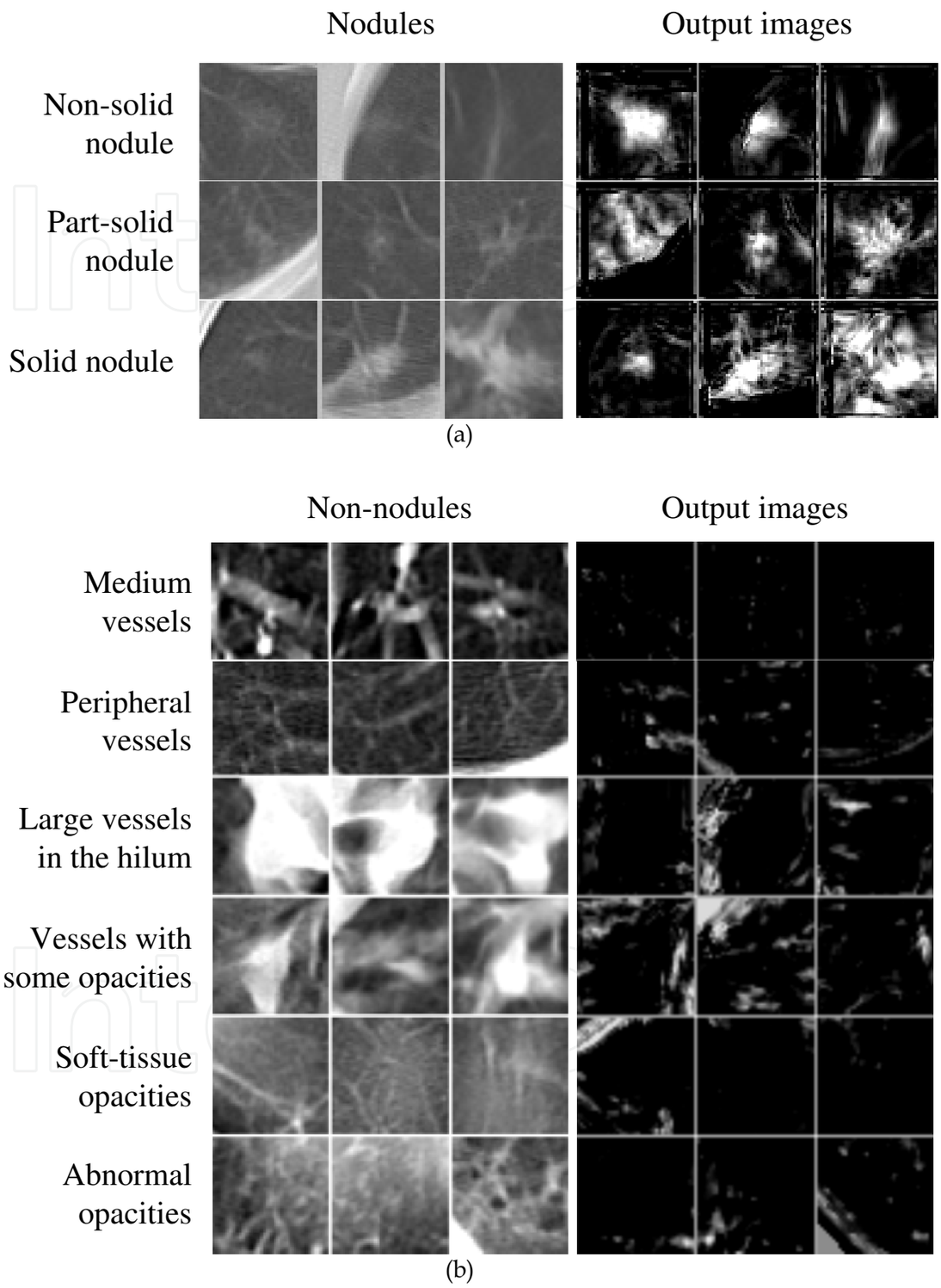

Fig. 7. Illustrations of various types of non-training nodules and non-nodules and corresponding output images of the trained MTANN. Nodules are represented by bright pixels, whereas non-nodules are almost dark around the centers of ROIs.

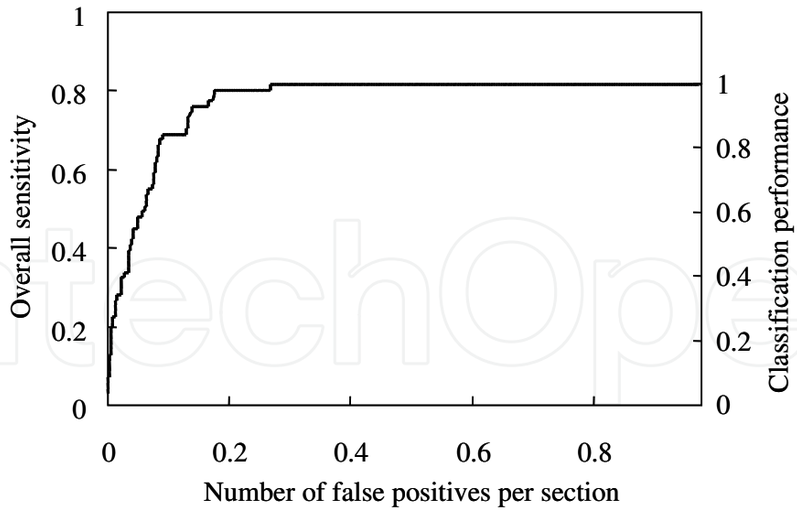

Fig. 8. FROC curve indicating the performance of the MTANN in distinction between 57 true positives (nodules) and 1.726 FPs (non-nodules).

2. Convolution NNs and shift-invariant NNs

Convolution NNs have been used for FP reduction in CAD schemes for lung nodule detection in CXRs (Lo, Lou et al. 1995; Lo, Chan et al. 1995; Lin, Lo et al. 1996). A convolution NN was trained with 28 chest radiographs for distinguishing lung nodules from non-nodules (i.e., FPs produced by an initial CAD scheme). The trained convolution NN reduced 79% of FP detections (which is equivalent to 2-3 FPs per patient), while 80% of true-positive detections were preserved. Convolution NNs have been applied to FP reduction in CAD schemes for detection of microcalcifications (Lo, Li et al. 2002) and masses (Sahiner, Chan et al. 1996) in mammography. A convolution NN was trained with 34 mammograms for distinguishing microcalcifications from FPs. The trained convolution NN reduced 90% of FP detections, which resulted in 0.5 FP detections per image, while a true-positive detection rate of 87% was preserved (Lo, Li et al. 2002).

Shift-invariant NNs have been used for FP reduction in CAD for detection of microcalcifications (Zhang, Doi et al. 1994; Zhang, Doi et al. 1996). A shift-invariant NN was trained to detect microcalcifications in ROIs. Microcalcifications were detected by thresholding of the output images of the trained shift-invariant NN. When the number of detected microcalcifications was greater than a predetermined number, the ROI was considered as a microcalcification ROI. With the trained shift-invariant NN, 55% of FPs was removed without any loss of true positives.

5. Advantages and limitations of PANN algorithms

As described earlier, the major difference between PANNs and ordinary classifiers is the direct use of pixel values with PANN. In other words, unlike ordinary classifiers, feature calculation from segmented objects is not necessary. Because the PANN can avoid errors caused by inaccurate feature calculation and segmentation, the performance of the PANN can potentially be higher than that of ordinary feature-based classifiers for some cases. PANNs learn pixel data directly, and thus all information on pixels should not be lost before the pixel data are entered into the PANN, whereas ordinary feature-based classifiers learn the features extracted from segmented lesions and thus important information can be lost

with this indirect extraction; also, inaccurate segmentation often occurs for complicated patterns. In addition, because feature calculation is not required for PANN, development and implementation of segmentation and feature calculation, and selection of features are unnecessary.

Ordinary classifiers such as linear discriminant analysis, ANNs, and support vector machines cannot be used for image processing, detection (localization) of objects, or enhancement of objects or patterns, whereas MTANNs can do those tasks. For example, MTANNs can separate bones from soft tissue in CXRs (Suzuki, Abe et al. 2006), and MTANN can enhance and detect lung nodules on CT images (Suzuki 2009).

The characteristics of PANNs which use pixel data directly should differ from those of ordinary feature-based classifiers. Therefore, combining an ordinary feature-based classifier with a PANN would yield a higher performance than that of a classifier alone or a PANN alone. Indeed, in previous studies, both classifier and PANN were used successfully for classification of lesion candidates into lesions and non-lesions (Zhang, Doi et al. 1994; Sahiner, Chan et al. 1996; Wei, Nishikawa et al. 1996; Zhang, Doi et al. 1996; Lo, Li et al. 2002; Suzuki, Armato et al. 2003; Arimura, Katsuragawa et al. 2004; Li, Arimura et al. 2005; Suzuki, Li et al. 2005; Suzuki, Yoshida et al. 2006; Suzuki, Yoshida et al. 2008; Suzuki, Rockey et al. 2010; Xu and Suzuki 2010 (in press); Suzuki, Zhang et al. in press).

A limitation of PANNs is the relatively long time for training because of the high dimensionality of input data. Because PANNs use pixel data in images directly, the number of input dimensions is generally large. For example, a 3D MTANN for 3D CT data requires 171 dimensions for its input (Suzuki, Yoshida et al. 2006; Suzuki, Yoshida et al. 2008). The ordinary feature-based classifiers are more efficient than PANNs. In an application of PANNs and feature-based classifiers to CAD schemes, a feature-based classifier should be applied first, because the number of lesion candidates that need to be classified is larger at an earlier stage. After the number of lesion candidates is reduced by use of the feature-based classifier, a PANN should be applied for further reduction of FPs. Indeed, previous studies employed this strategy (Suzuki, Armato et al. 2003; Arimura, Katsuragawa et al. 2004; Suzuki, Li et al. 2005; Suzuki, Yoshida et al. 2006; Suzuki, Yoshida et al. 2008; Suzuki, Rockey et al. 2010; Suzuki, Zhang et al. in press).

To address the issue of training time for PANN, dimensionality reduction methods for PANN have been proposed (Suzuki, Zhang et al. in press). With the use of the Laplacian-eigenfunction-based dimensionality reduction of the input vectors to a 3D MTANN, the training time was reduced by a factor of 8.5.

6. Conclusion

In this paper, PANNs were surveyed and compared with each other as well as with other non-PANN algorithms (i.e., ordinary feature-based classifiers) to make the similarities, differences, advantages, and limitations clear. The major difference between PANNs and non-PANN algorithms (e.g., classifiers) is a need for segmentation and feature calculation with non-PANN algorithms. The major advantage of PANNs over non-PANN algorithms is that no information is lost due to inaccurate segmentation and feature calculation, which would result in a higher performance for some cases such as complicated patterns. With the combination of PANNs with non-PANN algorithms, the performance of a system can be improved substantially. In addition to a classification task, MTANNs can be used for enhancement (and suppression) and detection (i.e., localization) of objects (or patterns) in images.

7. Acknowledgments

The authors are grateful to Ms. E. F. Lanzl for improving the chapter, to members in the Suzuki Laboratory in the Department of Radiology at the University of Chicago for their valuable contributions, and to my wife for editing this chapter. This work was partly supported by Grant Number R01CA120549 from the National Cancer Institute/National Institutes of Health and by the NIH S10 RR021039 and P30 CA14599.

8. References

[1] M. L. Giger and K. Suzuki, "Computer-Aided Diagnosis (CAD)," in *Biomedical Information Technology*, D. D. Feng, Ed.: Academic Press, 2007, pp. 359-374.

[2] K. Doi, "Current status and future potential of computer-aided diagnosis in medical imaging," *Br J Radiol*, vol. 78 Spec No 1, pp. S3-S19, 2005.

[3] A. Lostumbo, C. Wanamaker, J. Tsai, K. Suzuki, and A. H. Dachman, "Comparison of 2D and 3D views for evaluation of flat lesions in CT colonography," *Acad. Radiol.*, vol. 17, no. 1, pp. 39-47, 2010.

[4] K. Fukunaga, *Introduction to Statistical Pattern Recognition*, 2nd edition ed. San Diego: Academic Press, 1990.

[5] D. E. Rumelhart, G. E. Hinton, and R. J. Williams, "Learning representations by back-propagating errors," *Nature*, vol. 323, pp. 533-536, 1986.

[6] V. N. Vapnik, *The Nature of Statistical Learning Theory*. Berlin: Springer-Verlag, 1995.

[7] J. Shiraishi, Q. Li, K. Suzuki, R. Engelmann, and K. Doi, "Computer-aided diagnostic scheme for the detection of lung nodules on chest radiographs: localized search method based on anatomical classification," *Med. Phys.*, vol. 33, no. 7, pp. 2642-53, 2006.

[8] S. G. Armato, 3rd, M. L. Giger, and H. MacMahon, "Automated detection of lung nodules in CT scans: preliminary results," *Med. Phys.*, vol. 28, no. 8, pp. 1552-1561, 2001.

[9] H. Arimura, S. Katsuragawa, K. Suzuki, F. Li, J. Shiraishi, et al., "Computerized scheme for automated detection of lung nodules in low-dose computed tomography images for lung cancer screening," *Acad. Radiol.*, vol. 11, no. 6, pp. 617-629, 2004.

[10] M. Aoyama, Q. Li, S. Katsuragawa, H. MacMahon, and K. Doi, "Automated computerized scheme for distinction between benign and malignant solitary pulmonary nodules on chest images," *Med. Phys.*, vol. 29, no. 5, pp. 701-8, 2002.

[11] M. Aoyama, Q. Li, S. Katsuragawa, F. Li, S. Sone, et al., "Computerized scheme for determination of the likelihood measure of malignancy for pulmonary nodules on low-dose CT images," *Med. Phys.*, vol. 30, no. 3, pp. 387-94, 2003.

[12] Y. Wu, K. Doi, M. L. Giger, and R. M. Nishikawa, "Computerized detection of clustered microcalcifications in digital mammograms: applications of artificial neural networks," *Med Phys*, vol. 19, no. 3, pp. 555-60, 1992.

[13] Z. Huo, M. L. Giger, C. J. Vyborny, D. E. Wolverton, R. A. Schmidt, et al., "Automated computerized classification of malignant and benign masses on digitized mammograms," *Acad Radiol*, vol. 5, no. 3, pp. 155-68, 1998.

[14] H. Yoshida and J. Nappi, "Three-dimensional computer-aided diagnosis scheme for detection of colonic polyps," *IEEE Trans. Med. Imaging*, vol. 20, no. 12, pp. 1261-74, 2001.

[15] A. K. Jerebko, R. M. Summers, J. D. Malley, M. Franaszek, and C. D. Johnson, "Computer-assisted detection of colonic polyps with CT colonography using neural networks and binary classification trees," *Medical Physics*, vol. 30, no. 1, pp. 52-60, 2003.

[16] C. Muramatsu, Q. Li, R. A. Schmidt, J. Shiraishi, K. Suzuki, et al., "Determination of subjective similarity for pairs of masses and pairs of clustered microcalcifications on mammograms: comparison of similarity ranking scores and absolute similarity ratings," *Med. Phys.*, vol. 34, no. 7, pp. 2890-5, 2007.

[17] C. Muramatsu, Q. Li, R. Schmidt, K. Suzuki, J. Shiraishi, et al., "Experimental determination of subjective similarity for pairs of clustered microcalcifications on mammograms: observer study results," *Med. Phys.*, vol. 33, no. 9, pp. 3460-8, 2006.

[18] C. Muramatsu, Q. Li, K. Suzuki, R. A. Schmidt, J. Shiraishi, et al., "Investigation of psychophysical measure for evaluation of similar images for mammographic masses: preliminary results," *Med. Phys.*, vol. 32, no. 7, pp. 2295-304, 2005.

[19] H. Arimura, Q. Li, Y. Korogi, T. Hirai, S. Katsuragawa, et al., "Computerized detection of intracranial aneurysms for three-dimensional MR angiography: feature extraction of small protrusions based on a shape-based difference image technique," *Med Phys*, vol. 33, no. 2, pp. 394-401, 2006.

[20] K. Suzuki, I. Horiba, N. Sugie, and M. Nanki, "Neural filter with selection of input features and its application to image quality improvement of medical image sequences," *IEICE Trans. Inf. Syst.*, vol. E85-D, no. 10, pp. 1710-1718, 2002.

[21] K. Suzuki, I. Horiba, and N. Sugie, "Efficient approximation of neural filters for removing quantum noise from images," *IEEE Trans. Signal Process.*, vol. 50, no. 7, pp. 1787-1799, 2002.

[22] K. Suzuki, I. Horiba, and N. Sugie, "Neural edge enhancer for supervised edge enhancement from noisy images," *IEEE Trans. Pattern Anal. Mach. Intell.*, vol. 25, no. 12, pp. 1582-1596, 2003.

[23] K. Suzuki, I. Horiba, N. Sugie, and M. Nanki, "Extraction of left ventricular contours from left ventriculograms by means of a neural edge detector," *IEEE Trans. Med. Imaging*, vol. 23, no. 3, pp. 330-339, 2004.

[24] S. B. Lo, S. A. Lou, J. S. Lin, M. T. Freedman, M. V. Chien, et al., "Artificial convolution neural network techniques and applications for lung nodule detection," *IEEE Trans Med Imaging*, vol. 14, no. 4, pp. 711-8, 1995.

[25] S. C. B. Lo, H. P. Chan, J. S. Lin, H. Li, M. T. Freedman, et al., "Artificial convolution neural network for medical image pattern recognition," *Neural Networks*, vol. 8, no. 7-8, pp. 1201-1214, 1995.

[26] J. S. Lin, S. B. Lo, A. Hasegawa, M. T. Freedman, and S. K. Mun, "Reduction of false positives in lung nodule detection using a two-level neural classification," *IEEE Trans Med Imaging*, vol. 15, no. 2, pp. 206-17, 1996.

[27] S. C. Lo, H. Li, Y. Wang, L. Kinnard, and M. T. Freedman, "A multiple circular path convolution neural network system for detection of mammographic masses," *IEEE Trans Med Imaging*, vol. 21, no. 2, pp. 150-8, 2002.

[28] B. Sahiner, H. P. Chan, N. Petrick, D. Wei, M. A. Helvie, et al., "Classification of mass and normal breast tissue: a convolution neural network classifier with spatial domain and texture images," *IEEE Trans Med Imaging*, vol. 15, no. 5, pp. 598-610, 1996.

[29] S. Lawrence, C. L. Giles, A. C. Tsoi, and A. D. Back, "Face recognition: A convolutional neural-network approach," *IEEE Transactions on Neural Networks*, vol. 8, no. 1, pp. 98-113, 1997.

[30] C. Neubauer, "Evaluation of convolutional neural networks for visual recognition," *IEEE Transactions on Neural Networks*, vol. 9, no. 4, pp. 685-696, 1998.

[31] D. Wei, R. M. Nishikawa, and K. Doi, "Application of texture analysis and shift-invariant artificial neural network to microcalcification cluster detection," *Radiology*, vol. 201, pp. 696-696, 1996.

[32] W. Zhang, K. Doi, M. L. Giger, R. M. Nishikawa, and R. A. Schmidt, "An improved shift-invariant artificial neural network for computerized detection of clustered microcalcifications in digital mammograms," *Med Phys*, vol. 23, no. 4, pp. 595-601, 1996.

[33] W. Zhang, K. Doi, M. L. Giger, Y. Wu, R. M. Nishikawa, et al., "Computerized detection of clustered microcalcifications in digital mammograms using a shift-invariant artificial neural network," *Med Phys*, vol. 21, no. 4, pp. 517-24, 1994.

[34] K. Suzuki, S. G. Armato, 3rd, F. Li, S. Sone, and K. Doi, "Massive training artificial neural network (MTANN) for reduction of false positives in computerized detection of lung nodules in low-dose computed tomography," *Med. Phys.*, vol. 30, no. 7, pp. 1602-17, 2003.

[35] K. Suzuki, H. Yoshida, J. Nappi, and A. H. Dachman, "Massive-training artificial neural network (MTANN) for reduction of false positives in computer-aided detection of polyps: Suppression of rectal tubes," *Med. Phys.*, vol. 33, no. 10, pp. 3814-24, 2006.

[36] K. Suzuki, H. Abe, H. MacMahon, and K. Doi, "Image-processing technique for suppressing ribs in chest radiographs by means of massive training artificial neural network (MTANN)," *IEEE Trans. Med. Imaging*, vol. 25, no. 4, pp. 406-16, 2006.

[37] S. Oda, K. Awai, K. Suzuki, Y. Yanaga, Y. Funama, et al., "Performance of radiologists in detection of small pulmonary nodules on chest radiographs: effect of rib suppression with a massive-training artificial neural network," *AJR. Am. J. Roentgenol.*, vol. 193, no. 5, pp. W397-402, 2009.

[38] K. Suzuki, "A supervised 'lesion-enhancement' filter by use of a massive-training artificial neural network (MTANN) in computer-aided diagnosis (CAD)," *Phys. Med. Biol.*, vol. 54, no. 18, pp. S31-45, 2009.

[39] K. Suzuki, J. Shiraishi, H. Abe, H. MacMahon, and K. Doi, "False-positive reduction in computer-aided diagnostic scheme for detecting nodules in chest radiographs by means of massive training artificial neural network," *Acad. Radiol.*, vol. 12, no. 2, pp. 191-201, 2005.

[40] K. Suzuki, F. Li, S. Sone, and K. Doi, "Computer-aided diagnostic scheme for distinction between benign and malignant nodules in thoracic low-dose CT by use of massive training artificial neural network," *IEEE Trans. Med. Imaging*, vol. 24, no. 9, pp. 1138-1150, 2005.

[41] K. Suzuki, D. C. Rockey, and A. H. Dachman, "CT colonography: Advanced computer-aided detection scheme utilizing MTANNs for detection of "missed" polyps in a multicenter clinical trial," *Med. Phys.*, vol. 30, pp. 2-21, 2010.

[42] K. Suzuki, H. Yoshida, J. Nappi, S. G. Armato, 3rd, and A. H. Dachman, "Mixture of expert 3D massive-training ANNs for reduction of multiple types of false positives

in CAD for detection of polyps in CT colonography," *Med. Phys.*, vol. 35, no. 2, pp. 694-703, 2008.

[43] K. Suzuki, J. Zhang, and J. Xu, "Massive-training artificial neural network coupled with Laplacian-eigenfunction-based dimensionality reduction for computer-aided detection of polyps in CT colonography," *IEEE Trans. Med. Imaging*, in press.

[44] J.-W. Xu and K. Suzuki, "False-positive reduction in computer-aided detection of polyps in CT colonography: a massive-training support vector regression approach," in MICCAI Workshop on Computational Challenges and Clinical Opportunities in Virtual Colonoscopy and Abdominal Imaging, Beijing, China, 2010 (in press).

[45] F. Li, H. Arimura, K. Suzuki, J. Shiraishi, Q. Li, et al., "Computer-aided detection of peripheral lung cancers missed at CT: ROC analyses without and with localization," *Radiology*, vol. 237, no. 2, pp. 684-90, 2005.

[46] M. K. Ozkan, M. I. Sezan, and A. M. Tekalp, "Adaptive motion-compensated filtering of noisy image sequences," *IEEE transactions on circuits and systems for video technology*, vol. 3, no. 4, pp. 277-290, 1993.

[47] J. Canny, "A computational approach to edge detection," *IEEE Trans. Pattern Anal. Mach. Intell.*, vol. 8, no. 6, pp. 679-698, 1986.

[48] D. Marr and E. Hildreth, "Theory of edge detection," *Proceedings of the Royal Society of London. Series B, Biological Sciences*, vol. 207, no. 1167, pp. 187-217, 1980.

[49] M. H. Hueckel, "An operator which locates edges in digitized pictures," *Journal of the ACM (JACM)*, vol. 18, no. 1, pp. 113-125, 1971.

[50] Y. LeCun, B. Boser, J. S. Denker, D. Henderson, R. E. Howard, et al., "Backpropagation applied to handwritten zip code recognition," *Neural Comput.*, vol. 1, no. 4, pp. 541-551, 1989.

[51] K. Fukushima, "Neocognitron: a self organizing neural network model for a mechanism of pattern recognition unaffected by shift in position," *Biol Cybern*, vol. 36, no. 4, pp. 193-202, 1980.

[52] M. N. Gurcan, B. Sahiner, H. P. Chan, L. Hadjiiski, and N. Petrick, "Selection of an optimal neural network architecture for computer-aided detection of microcalcifications--comparison of automated optimization techniques," *Med Phys*, vol. 28, no. 9, pp. 1937-48, 2001.

[53] H. P. Chan, S. C. Lo, B. Sahiner, K. L. Lam, and M. A. Helvie, "Computer-aided detection of mammographic microcalcifications: pattern recognition with an artificial neural network," *Med Phys*, vol. 22, no. 10, pp. 1555-67, 1995.

[54] A. Hasegawa, K. Itoh, and Y. Ichioka, "Generalization of shift invariant neural networks: image processing of corneal endothelium," *Neural Networks*, vol. 9, no. 2, pp. 345-356, 1996.

[55] C. M. Bishop, "An example - character recognition," in *Neural Networks for Pattern Recognition*, C. M. Bishop, Ed. New York: Oxford University Press, 1995, pp. 1-4.

[56] D. F. Michaels, "Internal Organization of Classifier Networks Trained by Backpropagation," in *Neural Networks in Vision and Pattern Recognition*, J. Skrzypek and W. Karplus, Eds. Singapore: World Scientific, 1992.

[57] C. M. Bishop, "Neural Networks for Pattern Recognition." New York: Oxford University Press, 1995.

[58] R. O. Duda, P. E. Hart, and D. G. Stork, in *Pattern Recognition*, 2nd ed. Hoboken, NJ: Wiley Interscience, 2001, pp. 267-272.

[59] C. J. Murray and A. D. Lopez, "Mortality by cause for eight regions of the world: Global Burden of Disease Study," *Lancet*, vol. 349, no. 9061, pp. 1269-1276, 1997.

[60] G. E. Goodman, "Lung cancer. 1: prevention of lung cancer," *Thorax*, vol. 57, no. 11, pp. 994-999, 2002.

[61] J. H. Austin, B. M. Romney, and L. S. Goldsmith, "Missed bronchogenic carcinoma: radiographic findings in 27 patients with a potentially resectable lesion evident in retrospect," *Radiology*, vol. 182, no. 1, pp. 115-122, 1992.

[62] P. K. Shah, J. H. Austin, C. S. White, P. Patel, L. B. Haramati, et al., "Missed non-small cell lung cancer: radiographic findings of potentially resectable lesions evident only in retrospect," *Radiology*, vol. 226, no. 1, pp. 235-241, 2003.

[63] R. Glocker and W. Frohnmayer, "Uber die rontgenspektroskopische Bestimmung des Gewichtsanteiles eines Elementes in Gememgen und Verbindungen," *Ann. Physik.*, vol. 76, pp. 369-395, 1925.

[64] B. Jacobson and R. S. Mackay, "Radiological contrast enhancing methods," *Adv. Biol. Med. Phys.*, vol. 6, pp. 201-261, 1958.

[65] T. Ishigaki, S. Sakuma, Y. Horikawa, M. Ikeda, and H. Yamaguchi, "One-shot dual-energy subtraction imaging," *Radiology*, vol. 161, no. 1, pp. 271-273, 1986.

[66] T. Ishigaki, S. Sakuma, and M. Ikeda, "One-shot dual-energy subtraction chest imaging with computed radiography: clinical evaluation of film images," *Radiology*, vol. 168, no. 1, pp. 67-72, 1988.

[67] B. K. Stewart and H. K. Huang, "Single-exposure dual-energy computed radiography," *Med. Phys.*, vol. 17, no. 5, pp. 866-875, 1990.

[68] K. Doi, "Computer-aided diagnosis in medical imaging: Historical review, current status and future potential," *Comput. Med. Imaging Graph.*, vol. 31, no. 4-5, pp. 198-211, 2007.

[69] M. L. Giger, "Update on the potential role of CAD in radiologic interpretations: are we making progress?" *Acad. Radiol.*, vol. 12, no. 6, pp. 669-70, 2005.

[70] A. F. Frangi, W. J. Niessen, R. M. Hoogeveen, T. van Walsum, and M. A. Viergever, "Model-based quantitation of 3-D magnetic resonance angiographic images," *IEEE Trans. Med. Imaging*, vol. 18, no. 10, pp. 946-56, 1999.

[71] L. He, Y. Chao, K. Suzuki, and K. Wu, "Fast connected-component labeling," *Pattern Recognit.*, vol. 42, pp. 1977-1987, 2009.

[72] L. He, Y. Chao, and K. Suzuki, "A run-based two-scan labeling algorithm," *IEEE Trans Image Process*, vol. 17, no. 5, pp. 749-56, 2008.

[73] K. Suzuki, I. Horiba, and N. Sugie, "Linear-time connected-component labeling based on sequential local operations," *Comput. Vis. Image Underst.*, vol. 89, no. 1, pp. 1-23, 2003.

[74] P. C. Bunch, J. F. Hamilton, G. K. Sanderson, and A. H. Simmons, "A free-response approach to the measurement and characterization of radiographic-observer performance," *Journal of Applied Photographic Engineering*, vol. 4, pp. 166-171, 1978.

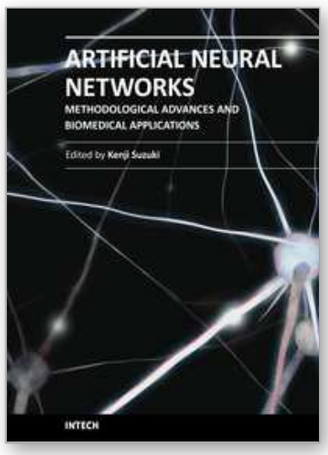

Artificial Neural Networks - Methodological Advances and Biomedical Applications

Edited by Prof. Kenji Suzuki

ISBN 978-953-307-243-2
Hard cover, 362 pages
Publisher InTech
Published online 11, April, 2011
Published in print edition April, 2011

Artificial neural networks may probably be the single most successful technology in the last two decades which has been widely used in a large variety of applications in various areas. The purpose of this book is to provide recent advances of artificial neural networks in biomedical applications. The book begins with fundamentals of artificial neural networks, which cover an introduction, design, and optimization. Advanced architectures for biomedical applications, which offer improved performance and desirable properties, follow. Parts continue with biological applications such as gene, plant biology, and stem cell, medical applications such as skin diseases, sclerosis, anesthesia, and physiotherapy, and clinical and other applications such as clinical outcome, telecare, and pre-med student failure prediction. Thus, this book will be a fundamental source of recent advances and applications of artificial neural networks in biomedical areas. The target audience includes professors and students in engineering and medical schools, researchers and engineers in biomedical industries, medical doctors, and healthcare professionals.

How to reference

In order to correctly reference this scholarly work, feel free to copy and paste the following:

Kenji Suzuki (2011). Pixel-Based Artificial Neural Networks in Computer-Aided Diagnosis, Artificial Neural Networks - Methodological Advances and Biomedical Applications, Prof. Kenji Suzuki (Ed.), ISBN: 978-953-307-243-2, InTech, Available from: http://www.intechopen.com/books/artificial-neural-networks-methodological-advances-and-biomedical-applications/pixel-based-artificial-neural-networks-in-computer-aided-diagnosis

INTECH
open science | open minds

InTech Europe
University Campus STeP Ri
Slavka Krautzeka 83/A
51000 Rijeka, Croatia
Phone: +385 (51) 770 447
Fax: +385 (51) 686 166
www.intechopen.com

InTech China
Unit 405, Office Block, Hotel Equatorial Shanghai
No.65, Yan An Road (West), Shanghai, 200040, China
中国上海市延安西路65号上海国际贵都大饭店办公楼405单元
Phone: +86-21-62489820
Fax: +86-21-62489821

IntechOpen